EUROPEAN ARC
ALMA Regional Centre || Italian

G353.2+0.9: Molecular gas and star formation in the vicinity of massive stars

A. Giannetti,*[1,2], J. Brand,[2], F. Massi[3], M. T. Beltrán[3] and A. Tieftrunk[4]
[1]**Dipartimento di Astronomia, Università di Bologna, Via Ranzani 1, 40127 Bologna, Italy**
[2]**INAF Istituto di Radioastronomia, CNR, Via Gobetti 101, 40129, Bologna, Italy**
[3]**INAF Osservatorio Astrofisico di Arcetri, Largo E. Fermi 5, 50125, Firenze, Italy**
[4]**Im Acker 21b, 56072 Koblenz, Germany**

G353.2+0.9 is an HII region in the NGC 6357 complex; its main ionization front is seen nearly edge-on. This is the ideal configuration to study the zone of interaction between the molecular gas and the energetic radiation and winds delivered by the numerous massive stars in the nearby cluster Pismis 24. I will discuss the morphology, temperature, mass and density of the gas in the PDR and its fragmentation along the ionization front, derived from low-angular resolution ($\sim 20'' - 50''$), single-dish observations.
Molecules with a sufficient amount of information could be analyzed by means of non-LTE calculations, with a Bayesian approach. We find that CN is indeed a good PDR tracer and that non-LTE calculations are essential to study the gas properties. We made maps of molecular abundances, dividing the column density maps of the molecule by that of H_2, derived from the 870 μm continuum. From these maps we see that the region near the ionization front always has lower abundances.
We are presently studying the star formation in G353.2+0.9 and in NGC 6357, by means of Spitzer IRAC, near-IR and X-ray data. We identify several star concentrations and young stellar objects in the region.

Secondo Workshop sull'Astronomia Millimetrica e Submillimetrica in Italia
April 2-3 2012
INAF - Istituto di Radioastronomia, Italian ARC, Bologna, Italy

*Speaker

© Copyright owned by the author(s) under the terms of the Creative Commons Attribution-NonCommercial-ShareAlike Licence.

1. Introduction

NGC 6357 is a complex of molecular clouds and HII regions, with still-ongoing star formation, nearly in the direction of the Galactic centre, at a distance of 2.56 kpc [7]. Fig. 1 (left) shows that gas and dust are distributed in a ring around a central cavity (or a collection of smaller, connected cavities).

The region of brightest emission at all wavelengths from radio to optical is G353.2+0.9, on which this study is focused. Fig. 1 (right) shows a zoom-in of this region as seen with HST. In G353.2+0.9 one can see clear features of obscuration due to dust, including an elephant trunk-like structure. This feature points South, where at a projected distance of 0.6 pc lies Pismis 24, a massive open cluster that contains 30-40 OB stars [12], and the main source of ionizing photons for G353.2+0.9. The location of the main ionization front (IF) is also indicated in Fig. 1 (right), appearing as an elongated region of bright optical (atomic lines) emission.

Before the availability of molecular observations, [3] suggested that the HII region was generated by a cluster of embedded sources rather than by the stars in Pismis 24, and that the cloud was ionization-bounded to the South. In this picture, the bright, elongated emission south of the elephant trunk (Fig. 1, right) was thought to be an ionization front. Molecular observations carried out by [8] did not support this claim, finding no molecular gas south of this feature.

Massive stars have a strong influence on the gas in their vicinity through energetic photons and winds, ionizing the gas, dissociating molecules and compressing and fragmenting the external layers of the clouds. The illumination of the clouds with such energetic photons makes the excitation conditions vary as a function of depth in the cloud. As a consequence, abundances of different molecules are expected to peak at different depths in the cloud, depending on the physical structure of the cloud itself and on its illumination, thus producing a chemical stratification. Within the cloud, the action of massive stars can both disrupt smaller structures such as clumps and cores, or can trigger their collapse, with a direct impact on star formation.

G353.2+0.9 is particularly suitable to study the influence of massive stars on the molecular gas, given the favorable orientation of its main ionization front, which is seen nearly edge-on. This configuration allows a simple study of phenomena such as fragmentation and chemical stratification, that are usually complicated by the presence of fore- and background material.

We are presently studying the star formation in the whole complex with Spitzer and Chandra archival data, with special attention to G353.2+0.9, for which we have JHK_s data. We want to investigate the properties of the stellar population and of the young stellar objects in Pismis 24 and in the PDR/HII region, determining their spatial distribution, mass and age. We will be able to study the role of Pismis 24 on the star formation in this region: are the massive stars triggering the birth of a new generation of stars, or are they dispersing the molecular cloud from which they were formed?

2. Fragmentation, Temperatures and Densities

We observed with the SEST several molecular transitions [$C^{18}O$(1-0), $C^{18}O$(2-1), CN(1-0), CN(2-1), CS(2-1), $C^{34}S$(2-1), CS(3-2), CS(5-4), $H_2CO(2_{1,2}$-$1_{1,1})$, SiO(5-4), CH_3CCH(6-5)], including optically thin tracers, temperature- and high-density tracers. We find that the molecular

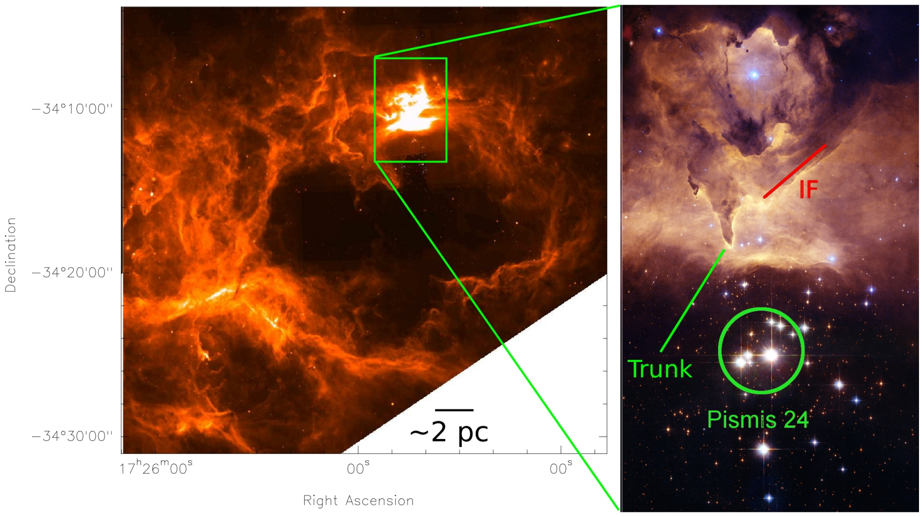

Figure 1: (Left): Spitzer IRAC (8 μm) image of NGC 6357, from the GLIMPSE survey (http://www.astro.wisc.edu/sirtf/; [1]). **(Right)**: HST image of G353.2+0.9 (hubblesite.org). The location of the ionization (IF) front, of the elephant trunk, and of the most massive stars in Pismis 24 are indicated.

gas is mostly to the north and behind the ionized gas, as already found by [8]. The gas associated to the HII region has a $V_{\rm LSR}$ between -10 and $+1$km s^{-1}. Figure 2 shows the integrated emission of CS(5−4), observed at the highest angular resolution ($\sim 21''$). The molecular gas appears to be associated with both the elephant trunk and the ionization front. However, molecular lines also give information on the radial velocity of the gas with respect to the observer, allowing us to identify clumps that are spatially distinct, but indistinguishable in projection. Thus, we decomposed the emission profiles in Gaussian components, starting from optically thin tracers. The emission of such molecules traces the column density. In this way, we identified 14 clumps, showing that the gas appears already fragmented at the low resolution of single-dish observations [4].

Using the ratio of two optically thin transitions of the same molecule and assuming LTE, one can derive the temperature of the gas. In our case, we used the C^{18}O(2−1)/C^{18}O(1−0) ratio. We find excitation temperatures typically in the range between 15 and 20 K, with maxima and minima around 25-30 and 10 K, respectively. We find that the clumps aligned along the ionization front are characterized by a slightly higher temperature than the others. We derived a temperature for all points in our map with a clear detection, thus obtaining temperatures at several locations for a single clump. In some cases clumps show a T-minimum toward their projected centre, indicating that in these clumps the internal layers are colder, as expected in the case of external heating.

Symmetric-top molecules are efficient temperature tracers, because different K-ladders are connected only through collisions, and the population of each K-ladder depends only on kinetic temperature [2]. CH_3CCH is a symmetric-top molecule with a relatively low dipole moment, so it should have a thermalized level population in the dense cores of molecular clouds [2]. Assuming that the emission of CH_3CCH is optically thin, the temperature can be estimated through a so-called rotation diagram (or Boltzmann plot) [5]. For the clump associated with the elephant trunk,

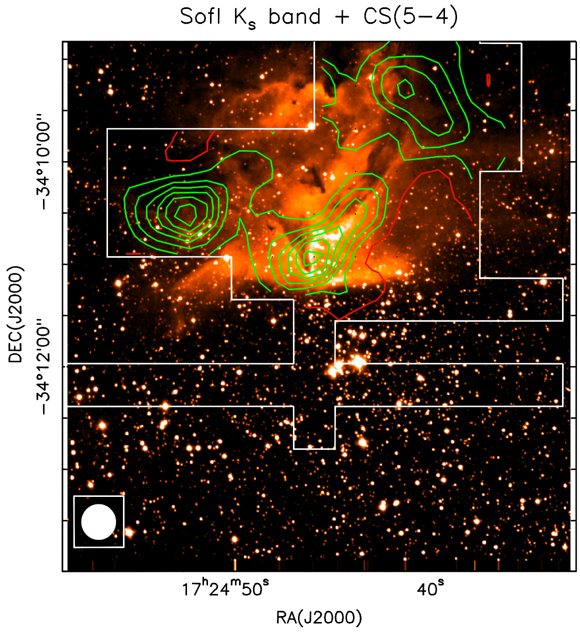

Figure 2: Integrated emission of CS(5−4) (contours; $-10, 0$km s^{-1}) superimposed on our SofI K$_s$ band image (Massi et al, in prep.). The 3σ contour is shown in red. The beam and the observed region are indicated in white.

the temperature derived in this way is higher that that derived from $C^{18}O$, showing that in this case the high-density layers are hotter, possibly due to the presence of internal heating sources.

We calculated the column density and mass for the clumps in this region, with the temperature of the gas derived from $C^{18}O$. In a simple stability analysis we compared the virial masses of the clumps, for a $1/r^2$ density profile, with their LTE masses. All the clumps with masses $M \gtrsim 50M_\odot$ appear to be dominated by gravity; these have $M_{vir}/M_{LTE} \lesssim 1$. On the other hand, clumps with small masses have high values of the ratio M_{vir}/M_{LTE}, i.e. these are probably being dissociated by the destructive action of the massive stars in Pismis 24.

The molecules with a sufficient amount of information available (CS: 3 transitions + 1 transition of $C^{34}S$; CN: 2 transitions with hyperfine structure) could be analyzed with non-LTE calculations [4]. Non-LTE calculations are essential to derive physical properties of the gas from certain molecules, depending on the excitation conditions. Assuming LTE, the values of the temperature, column and volume densities can be significantly different, even by orders of magnitude. We used RADEX[1] [10] to build a large grid of models, characterized by the parameters T_K, n_{H_2} and N_{mol} (kinetic temperature, volume density of H_2, and column density of the molecule analyzed). To compare observations with the model results, we estimate the brightness temperature of the lines assuming the source size as determined from CS(5−4), which is the transition observed with the highest angular resolution. We considered Gaussian uncertainties on line temperatures (CS), fluxes and optical depth (CN), as given from the fit of the emission lines, performed with CLASS. To analyze the results we used a Bayesian approach, assigning to each model a probability given by

[1] http://www.strw.leidenuniv.nl/∼moldata/radex.html

the Bayes theorem:

$$P(T_{\rm K}, N_{mol}, n_{\rm H_2}|{\rm data}) = \frac{1}{\varphi} P({\rm data}|T_{\rm K}, N_{mol}, n_{\rm H_2}) P(T_{\rm K}, N_{mol}, n_{\rm H_2}),$$

where $P(T_{\rm K}, N_{mol}, n_{\rm H_2}|{\rm data})$ is the probability of the model with parameters $T_{\rm K}$, N_{mol} and $n_{\rm H_2}$, given the data (called the "posterior"); $P({\rm data}|T_{\rm K}, N_{mol}, n_{\rm H_2})$ is the probability of obtaining the data measured, given the model (the "likelihood"), $P(T_{\rm K}, N_{mol}, n_{\rm H_2})$ is the *a priori* probability of the parameters that characterize the model (the "prior"), and φ is a normalization factor. The "prior" includes what we already know of these quantities, *before* the observations that we are analyzing. We assumed a constant prior for CS (i.e. all the value of $T_{\rm K}$, N_{mol} and $n_{\rm H_2}$ are equally probable, a priori), while for CN we considered a Gaussian prior on $T_{\rm K}$, with mean $\mu = 35$ K and $\sigma = 30$ K, useful to reduce the degeneration at high temperatures. The assumed prior is consistent with all the other temperature tracers for this region ($C^{18}O$, CH_3CCH, CO and CS).

The Bayesian approach is particularly powerful for the parameter estimation, so we decided to use it to derive the probability distribution of the model parameters, i.e. to constrain the physical properties of the gas and their uncertainties. The column density of the molecule has much more stringent constraints than $n_{\rm H_2}$ or $T_{\rm K}$, given by our measure of τ from the CS(2−1)/$C^{34}S$(2−1) ratio or from the ratio of the CN hyperfine satellite components ratio. The analysis shows that the kinetic temperature probed by CS is slightly lower than that probed by CN (typically $20-30$ K vs. $30-40$ K). A similar behaviour is found for $n_{\rm H_2}$, with average values a factor of 5 greater for CN ($\sim 5\times10^5$ cm^{-3}).

3. Molecular Abundances

We constructed maps of molecular column density for G353.2+0.9. The ATLASGAL[2] [9] image at 870 µm allowed us to derive a map of column density of molecular hydrogen, assuming a dust temperature $T_d = 30$ K and greybody emission for the dust. Thus, we were able to derive maps of molecular abundance for the observed species, dividing their column density maps by that of H_2, smoothed to the same resolution (Fig. 3). The maps allowed us to investigate how the molecular abundances vary across the region. A common pattern is visible in Fig. 3: the abundances tend to be lower near the IF and the elephant trunk, the regions most exposed to the radiation of the massive stars of Pismis 24. On average, abundances are lower by a factor of 2, showing that, most likely, these molecules are being dissociated here.

Having derived the column density for CN with the non-LTE analysis, we constructed an abundance map (Fig. 4), like those derived for the other molecules. We still find a lower abundance in the region near the elephant trunk and the IF, but with smaller variation with respect to the other molecules studied. This is expected if CN traces the hot, compressed, surface layers of the PDR, where its abundance is increased.

Given the large quantity of energetic photons, we expect selective photodissociation to have an impact on the column density of different isotopologues. The line ratios of ^{13}CO and $C^{18}O$ show a relative increase in abundance of the former at the edge of clumps along the IF toward Pismis

[2]http://www.mpifr-bonn.mpg.de/div/atlasgal/

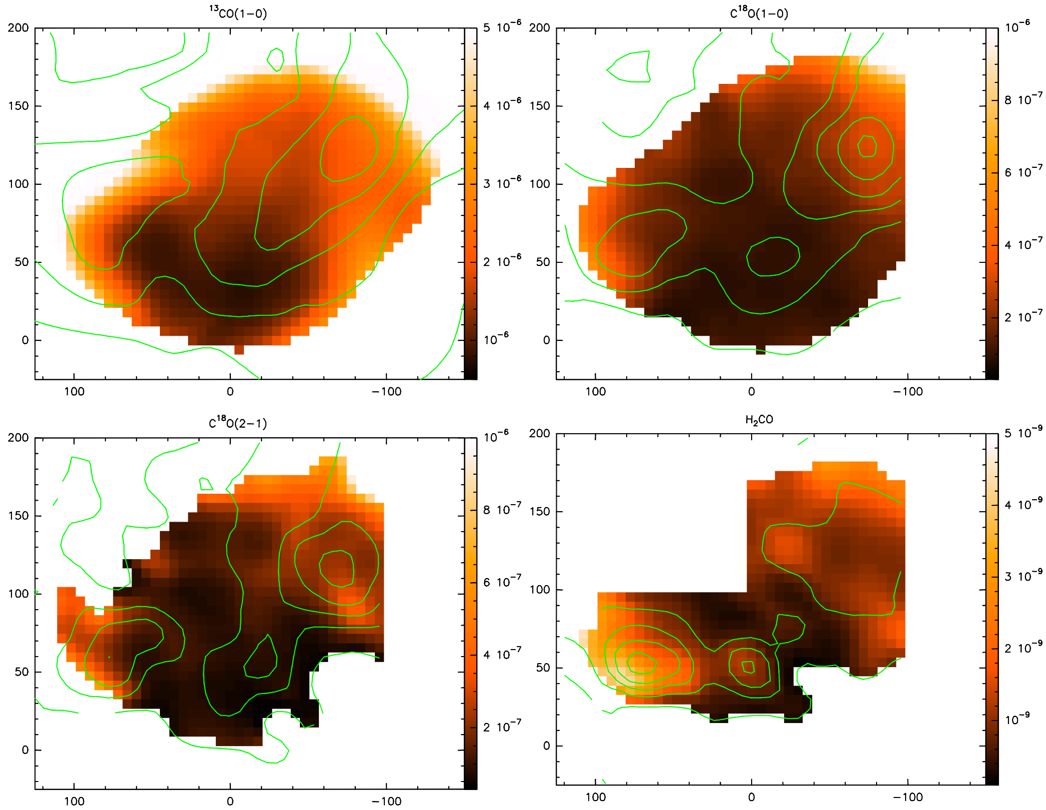

Figure 3: Column density contours (green) of the molecule specified above each panel, superimposed on molecular abundance maps (greyscale). The values of the molecular abundance are shown in the wedge beside each panel.

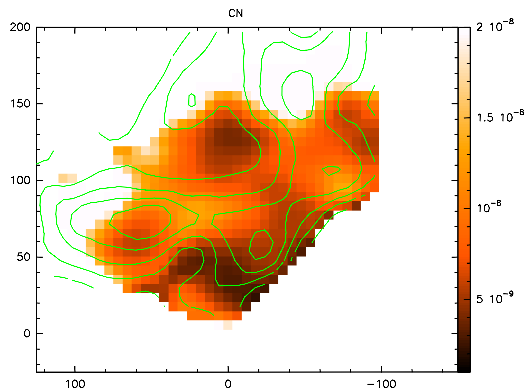

Figure 4: Column density contours (green) of the CN, superimposed on molecular abundance maps (greyscale). The values of the molecular abundance are shown in the wedge beside the panel.

24. [11] made a grid of PDR models predicting the column density of the CO isotopologues as a function of depth in the cloud. The models require as input the flux of UV photons impacting on the cloud, which was estimated considering the three brightest stars in Pismis 24, namely two of spectral types O3.5 and an O4. Comparing our measured values for the relative abundance of ^{13}CO and C^{18}O, with those of the model, we find that the observations can be explained in terms of selective photodissociation, for values of visual extinction, volume density and UV flux typical of G353.2+0.9.

4. Future Work

ALMA is the ideal tool to study chemical stratification and the gas properties at arcsecond resolution. Even with short exposures the UV-coverage is very good, and it offers the possibility to observe simultaneously several molecules and transitions. These can be modeled in detail to derive the physical properties of the gas at each location in the map allowing one to study the chemical stratification in the PDR.

Given the high degree of fragmentation of the gas already visible at the angular resolution of a single-dish, we requested and obtained time at the EVLA to observe ammonia (an efficient tracer of high-density gas) in this region, in CnB configuration. This will allow us to reach an angular resolution of $\sim 1\farcs5$, sufficient to study in detail the structure of the gas along and across the IF and the elephant trunk, to study the small-scale ordered motions *of* and *in* the clumps, and to evaluate the impact thereon of newly-formed, still embedded stars.

5. Star Formation

To study the star formation in the whole complex, we constructed Spitzer mosaics in the 4 IRAC bands (3.6 μm, 4.5 μm, 5.8 μm, 8.0 μm; Project ID 20726 "Spitzer follow-up of HST observations of star formation in HII regions", P.I. Jeff Hester), much deeper than those of the GLIMPSE [1] survey. In Fig. 5 we show a composite three colour image of the NGC 6357 complex, made with 3 of the 4 IRAC bands. We derived maps of the surface density of stars, and identified several stellar concentrations (Massi et al., in prep). These are found at the location of Pismis 24 and in its surroundings, along the dust ring visible in Fig. 1, and near the center of the cavity (Fig. 6). It is tempting to identify this last group of stars as the remnant of a cluster older than Pismis 24, possibly responsible of shaping the cavity.

We constructed colour-colour diagrams to recognize PAH contamination [6], and correct for it when identifying the young stellar objects (YSO) in the region. Several class I and II objects are identified across NGC 6357, mainly at the location of the stellar concentrations and along the molecular/dusty ring visible in Fig. 1.

For G353.2+0.9 we also have SofI JHK$_s$ images, which we will combine with Spitzer and X-ray (Chandra) data, to investigate the properties of the massive stars of Pismis 24 and how they influence the star formation in the region. The combined action of the ionizing radiation and stellar winds may accumulate and compress the molecular gas; the overdense regions might become unstable and collapse to form new stars, leading to a concentration of YSOs near the IF.

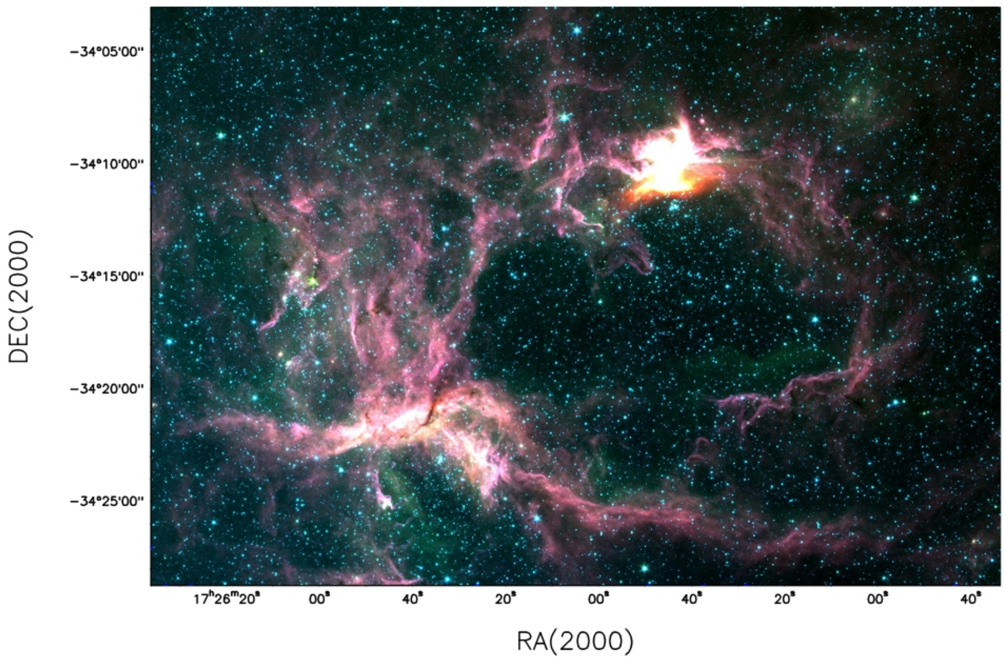

Figure 5: Three color image (red: 8.0 μm, green: 4.5 μm, blue: 3.6 μm) of the NGC 6357 complex obtained with all the Spitzer data available.

From the K luminosity function, we constructed the initial mass function (IMF) (Massi et al., in prep.) for Pismis 24, which is consistent with a Salpeter IMF. Preliminary results indicate the presence of hundreds of objects with near-IR excess, associated both to Pismis 24 and to G353.2+0.9. This shows that there is still a population of stars with circumstellar disks, despite the strong irradiation from the massive stars. The fraction of stars with a disk will give us a handle on the age of the cluster.

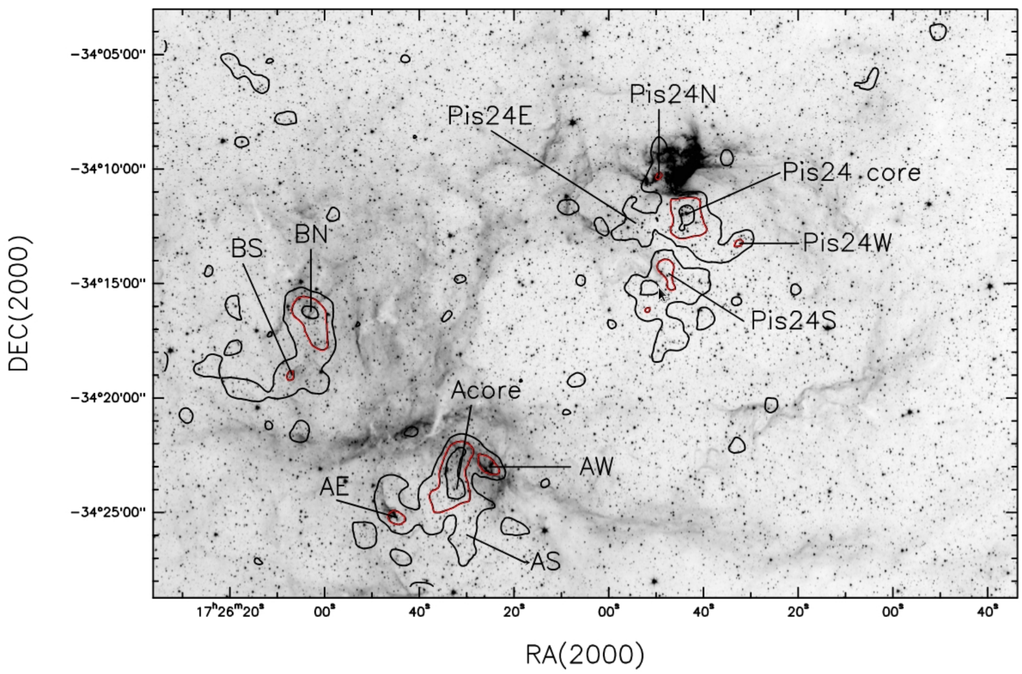

Figure 6: Contour map of the surface density of IRAC sources, counted in squares of $1' \times 1'$, displaced by $30''$. The contours start from the mean stellar surface density plus 3σ, in steps of 3σ, and are superimposed on the 3.6 μm image. The tentatively identified subclusters are also labeled.

6. Summary

We observed G353.2+0.9, an HII region in the NGC 6357 complex, in several molecular transitions, performing both LTE and non-LTE analyses to derive the physical properties of the gas. In summary, we find that:

- The gas appears already significantly fragmented at the relatively low resolution ($\sim 21-50''$) of single-dish observations.
- The molecular gas has temperatures in the range $\sim 10-50$ K, and volume densities from $\sim 10^3$ cm^{-3} ($C^{18}O$) to $\sim 10^6$ cm^{-3} (CN), with higher values of both parameters in the surface layer of the PDR and along the IF.
- Comparing virial and LTE masses we find that clumps with $M \gtrsim 50 M_\odot$ are dominated by gravity. Less massive clumps are presumably suffering the destructive influence of the stars of Pismis 24.
- We find that CN is indeed a good PDR tracer, with a substantial part of its emission coming from the hotter, compressed surface layers of the cloud.
- For the analysis of molecules such as CS and CN, non-LTE calculations are fundamental to infer the gas physical properties. The Bayesian approach is particularly powerful for this.

- We obtained maps of the molecular abundances in this region. We find that molecular abundances are always lower in the region near the IF, toward Pismis 24.
- Selective photodissociation can explain the anomalous ^{13}CO/C^{18}O line ratios found in the region of the IF and the elephant trunk, toward Pismis 24.
- We identified several concentrations of stars and a significant number of YSOs, in the NGC 6357 complex.
- Near IR data indicate that Pismis 24 has a Salpeter IMF, and that a sizable population of stars with a circumstellar disk is still present in the cluster and in the PDR/HII region.

References

[1] Benjamin, R. A., Churchwell, E., Babler, B. L., et al. 2003, PASP, 115, 953

[2] Bergin, E. A., Goldsmith, P. F., Snell, R. L., & Ungerechts, H. 1994, ApJ, 431, 674

[3] Felli, M., Persi, P., Roth, M., et al. 1990, A&A, 232, 477

[4] Giannetti, A., Brand, J., Massi, F., Beltrán, M.T & Tieftrunk, A., 2012, A&A, 538, A41

[5] Goldsmith P. F. & Langer W. D. 1999, ApJ, 517, 209

[6] Gutermuth, R. A., Megeath, S. T., Myers, P.C., et al. 2009, ApJS, 184, 18

[7] Massey, P., DeGioia-Eastwood, K., & Waterhouse, E. 2001, AJ, 121, 1050

[8] Massi, F., Brand, J., & Felli, M. 1997, A&A, 320, 972

[9] Schuller, F., Menten, K. M., Contreras, Y., et al. 2009, A&A, 504, 415

[10] van der Tak, F. F. S., Black, J. H., Schöier, F. L., Jansen, D. J., & van Dishoeck, E. F. 2007, A&A, 468, 627

[11] Visser, R., van Dishoeck, E. F., & Black, J. H. 2009, A&A, 503, 323

[12] Wang, J., Townsley, L. K., Feigelson, E. D., et al. 2007, ApJS, 168, 100